CONTROL OF REAR-WHEEL STEERING FOR A FOUR-WHEEL STEERED AGRICULTURAL STANDARD TRACTOR

Ruben Hefele[1]*, Johannes Burth[1], Michael Maier[1], Timo Oksanen[1,2]

[1]*Chair of Agrimechatronics, Technische Universität München, Dürnast 8, 85354 Freising*
[2]*Munich Institute of Robotics and Machine Intelligence (MIRMI), Technische Universität München, Georg-Brauchle-Ring 60-62, 80992 München*

* Corresponding author: Tel.: +49 (8161) 71-4903; E-mail address: ruben.hefele@tum.de

ABSTRACT

Steering is crucial for automation in agriculture. Four-wheel steered tractors are better suited for highly automated agricultural machinery compared to front-wheel steered tractors. Common tractors with four-wheel steering have equal large tire diameters on the front and rear axles. In comparison, this study uses a standard tractor, which means that the tires of the rear axle have a larger diameter than the tires of the front axle, thus significantly affecting the rear-axle steer control. An off-the-shelf front-wheel steering system is used, while the rear-wheel steering control is built from scratch. Steady-state accuracy and fast convergence are the control objectives. A double-acting differential cylinder is used as a steering actuator, supplied by a current controlled proportional directional valve with feedback from an angle sensor. The tractor's load sensing variable displacement pump provides hydraulic power. A SIL2 functional safety variant electric control unit with redundancy is used for the rear-axle controller. In-vehicle network communication is via CAN bus based on SAE J1939. System identification and modelling of the steering system are carried out, followed by controller setup and tuning using first order lag plus integrator plus delay rules while considering dead-zone and valve saturation. Further on, this paper introduces two novel controller designs, utilizing gain scheduling and model-based state space control techniques, which lead to enhanced performance.

Keywords: four-wheel steering, servo hydraulic control, system identification, highly automated agricultural machinery, FOLIPD process, gain scheduling , 2DOF control, PID control

1. INTRODUCTION

Highly automated tractors have emerged as a promising solution in modern agricultural practices, providing efficient and precise operations without relying on human intervention. These advanced machines combine the power of automation, navigation systems, and sophisticated control algorithms to carry out various tasks. Among the critical aspects of achieving effective autonomous operation, precise control over the tractor's heading plays a pivotal role in ensuring accurate trajectory tracking and manoeuvrability.

In many agricultural scenarios, especially on sloping terrains, maintaining the desired heading of the tractor and implement becomes particularly challenging due to inherent disturbances and variations in ground conditions. Conventional tractors typically rely solely on front axle steering mechanisms, resulting in limited control capabilities and reduced stability, especially under side slip conditions. However, integrating rear-axle steering into the control system provides an innovative solution to these challenges, allowing dynamic control of the tractor's heading and compensating for side slip at slopes. Likewise, when considering mounted implements, it is important to consider the precise tracking of paths in curves and the kinematic constraints to avoid placing excessive mechanical strain on the mounting links.

In our research-tractor project “AMX G-trac”, we have modified and customized a four-wheel steerable standard tractor to perform in future highly automated field operations. While the base tractor is built by Traktorenwerk Lindner, Austria, the rear-wheel system was redeveloped to enable more accurate steering servo control than the original system was able to perform. The new system is based on the original valves and a Parker IQAN mobile control system. Newly developed control algorithms compensate for system nonlinearities and provide smooth actuation. In contrast, the front-wheel steering is based on the Danfoss electro-hydraulic steering valve.

The paper presents two system identification methods in section **3.1** and **3.2**. While the first is a state of the art method, the second is a novel proposal, representing the system to a more precise extend. In the subsequent stage a systematic design approach for a PD controller with first order lag plus integrator plus delay (FOLIPD) tuning rules (section **4.1**), a two-degree-of-freedom (2DOF) controller combining model-based state space control and PD control (section **4.2**) as well as a gain scheduled PD controller (section **4.3**) is described. The gain scheduling controller shows better performance.

2. ELECTROHYDRAULIC STEERING SYSTEM

The problem analysed in the present work is the steering servo control of a tractor for future autonomous operation. **Figure 1** depicts the composition of the steering system, comprising electric control units (ECUs) and sensors. The hydraulic system of the tractor is based on a load-sensing circuit. Double-acting differential cylinders are actuated through directional proportional valves in order to realize different steering angles.

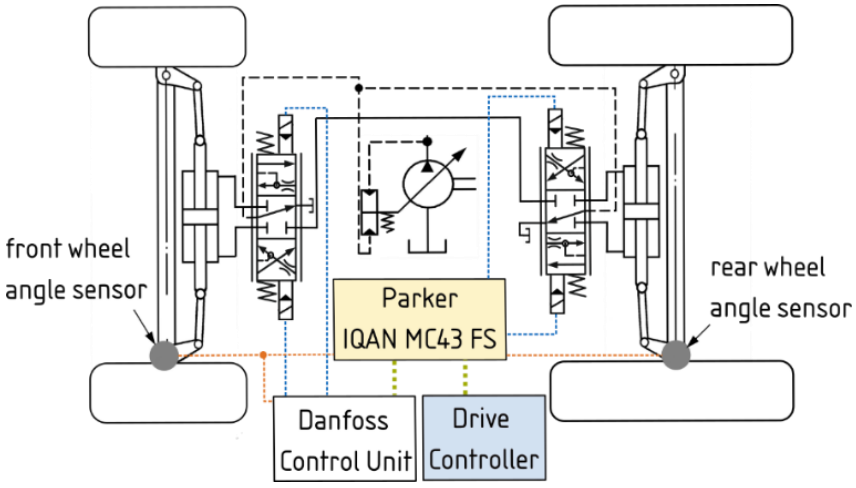

Figure 1: Simplified steering system

For control of the front-axle steering the built-in Danfoss system is utilized via CAN bus-based J1939 communication. To simplify the illustration, the manual steering system is omitted from **Figure 1**.

The Parker IQAN controller serves as a gateway between the main drive controller and the tractor system to control both, rear and front steering angles, which enables functional safe operation. The IQAN MC43 FS is a rugged master controller providing multiple CAN bus channels, analog, digital and PWM in- and outputs as well as SIL2 safety features.

Programming of the IQAN is facilitated by IQANdesign, a high-level graphical design tool that also supports MATLAB Simulink model import. The IQAN controller is directly used for rear-axle control, accomplished through two PWM outputs that command the directional proportional valve. Additionally, lock valves (which are not displayed) are controlled by the IQAN. The analog voltage input from the rear wheel angle sensor serves as control feedback. The IQAN has a built-in PWM current controller, delivering a precision of 1 mA, while the operating range is from roughly -2500 to 2500 mA. To calibrate the wheel angle sensors, accurate values for the true steering angle were

measured using a total station and subsequently mapped to the sensor voltage outputs within IQANdesign.

3. PROCESS MODEL AND SYSTEM IDENTIFICATION

In the present work a FOLIPD process model (1) is used for modeling the hydraulic rear steer plant. Literature shows that this model is acceptably accurate to approximate the servo-valve dynamics [1]. Utilizing the FOLIPD process model is also suggested in [2–5].

$$G(s) = \frac{1}{s} \cdot \frac{K_v}{1 + T_F\, s} e^{-sL} \tag{1}$$

The transfer function consists of an integrator part, an open-loop transform function between valve current input and cylinder speed output as well as an input-output time delay. K_v represents the process gain, T_F the time constant and L the process time delay.

To ensure consistent results in system identification, the tractor was lifted so that the tires didn't have ground contact while measurements were taken. This was done to maintain a constant load profile and under the assumption that the tractor's steering behavior during this setup closely resembles its steering behavior during actual field operations. Measurements were taken with a sample rate of 50 ms.

3.1. Model identified from open-loop step response

While the identification can be performed utilizing an impulse response [5], in the first approach of the present work for model identification a step response procedure is used as suggested in [6].

First, the dead zone of the valve must be determined using a ramp input signal as presented in **Figure 2**. It can be expressed as follows:

$$u_{dz}(t) = \begin{cases} u(t), & if\ u(t) \geq u_{dz,+} \\ 0, & if\ u_{dz,-} < u(t) < u_{dz,+} \\ u(t), & if\ u(t) \leq u_{dz,-} \end{cases} \tag{2}$$

Where negative dead zone limit $u_{dz,-} = -850\ mA$ and positive limit $u_{dz,+} = 965\ mA$.

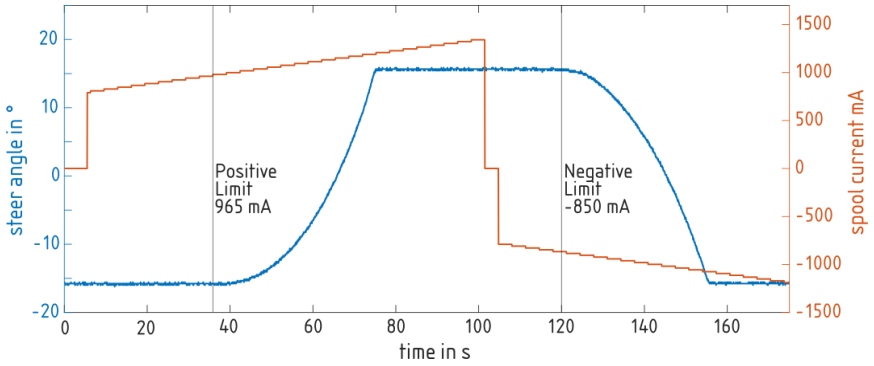

Figure 2: Dead zone investigation

In the subsequent stage, the nonlinear process gains are determined. In order to achieve plug-and-play tuning between the tractor and implement, Oksanen [6] suggests increasing the step in increments of 10%. However, since there is no need for plug-and-play functionality in the rear-axle control and a more precise resolution of the nonlinear process gains is preferred, we have chosen to use increments of 2%.

Figure 3 illustrates the step input with 2% increments, starting from the dead zone and rising to a maximum of 2500 mA, which corresponds to 100% spool current. By determining the steady-state speed for each operating point, **Figure 4** is generated. This figure considers both the dead zone and the saturation, with a negative saturation level of 2386 mA and positive saturation level of 2234 mA.

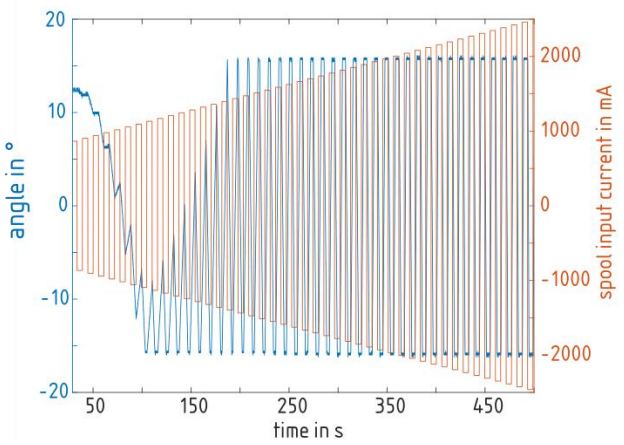

Figure 3: Spool current and steer angle

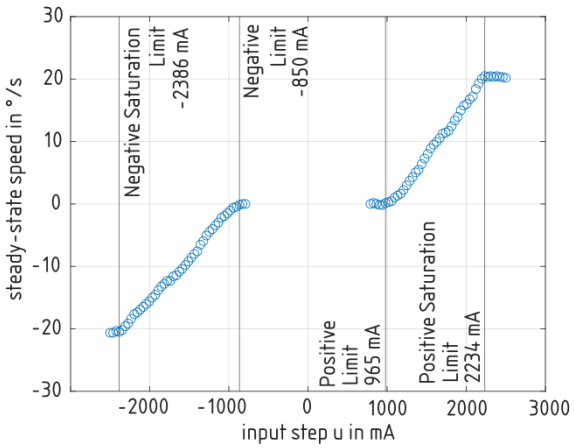

Figure 4: Steady-state speed versus spool current

As observed in **Figure 3**, it is evident that the allowable steering angle is confined within a range of 16 degrees in both the positive and negative directions.

The time delay L and time constant T_F are identified from six step responses (three positive, three negative) and averaged. An exemplary step response for integrating processes and the time delay L and time constant T_F is presented in **Figure 5**.

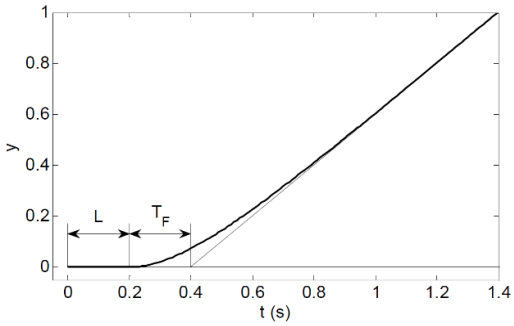

Figure 5: Step response for integrating process with delay L and time constant T_F [6]

Chosen operating points were 55 %, 75 % and 95 % of respective saturation limit to calculate the averaged parameters.

(3) presents the identified model:

$$G(s) = \frac{1}{s} \cdot \frac{K_v}{1 + 0.0385\,s} e^{-0.2658\,s} \tag{3}$$

The process gain K_v is non-constant due to the nonlinear process, which is why averaging K_v would not adequately reflect the process. In the MATLAB Simulink model a look-up table is used between plant and transfer function input to represent the nonlinear process gain incorporating both the dead zone and the saturation, presented by **Figure 6** which is a polished version of **Figure 4.** This means

that any currents exceeding the saturation limit have been eliminated, and currents within the dead zone have been set to zero.

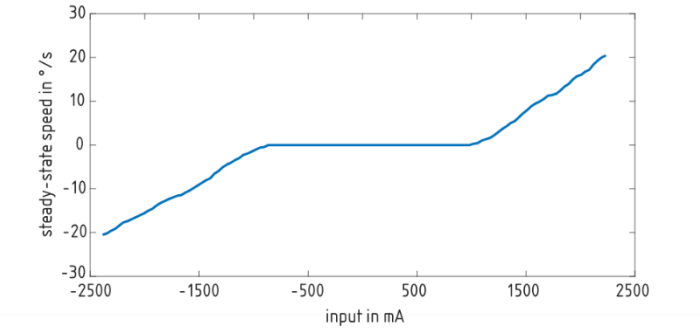

Figure 6: Look-up table for nonlinear process gain K_v including dead zone and saturation

3.2. Greybox modelling with time-varying delay and time constant

In an alternative modelling approach, greybox identification was investigated as proposed by Galuppini et al. [7]. They propose to inject a series of sinusoidal inputs at different frequencies to the plant. However, it was observed that the resulting transfer function deviated considerably from the transfer function stated in (3), indicating nonlinearities in addition to the dead zone and saturation. Consequently, a different input-output method was employed.

In this study, the greybox system was stimulated with various step inputs, and the measured angle was recorded as the output, similar to the procedure outlined in **Figure 3**. (1) served as the underlying model for this investigation. With 50 operating points in both the negative and positive directions, a total of 100 different transfer functions result, varying in process gain K_v, time constant T_F and delay L. **Figure 7** depicts the resulting varying process gain. A double exponential curve was fitted to the positive and negative directions, to obtain continuous monotone behaviour.

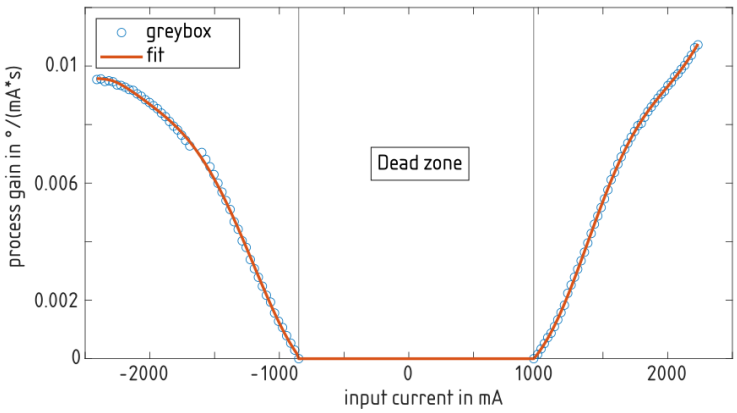

Figure 7: Time-varying process gain identified from greybox

Figure 8 and **Figure 9** present the time-varying time constant and delay identified with greybox modelling. The measurement values for the time constant exhibit considerable scattering, while the delays demonstrate exponential growth towards the dead zone with less scattering. To account for this, an averaged value is adopted for the time constant (**Figure 8**), distinguishing between positive and negative spool displacements. Within the dead zone, a linear interpolation is employed, as no significant impact on the simulated valve behaviour is observed.

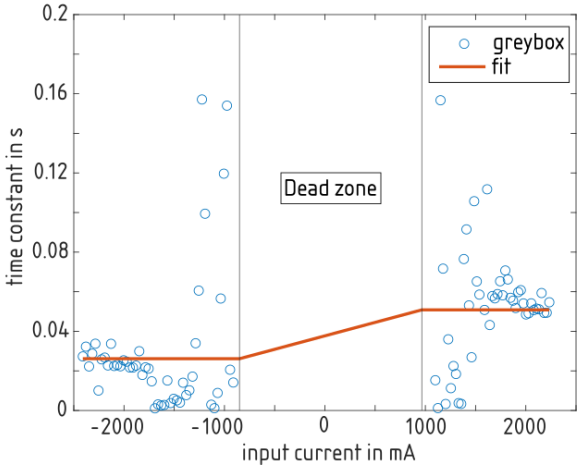

Figure 8: Time-varying time constant identified from greybox

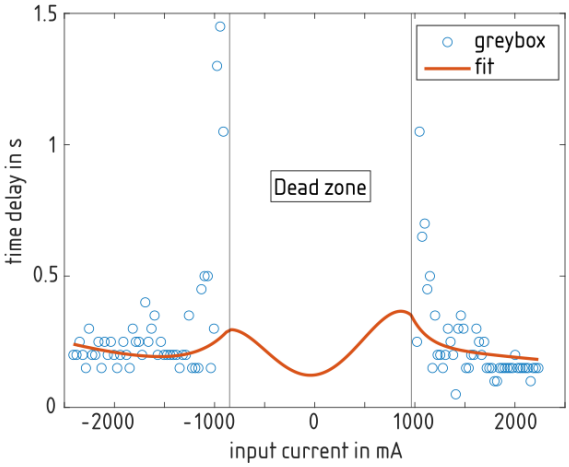

Figure 9: Time-varying delay identified from greybox with fitted polynomial to dead zone to consider the delay at 0 mA while maintaining continuous behaviour

For the delay (**Figure 9**), double exponential curves are fitted to both positive and negative spool displacements outside of the dead zone, ensuring a continuous and monotonic behaviour. In contrast, the delay for the transition to 0 mA currents differs significantly from delays for currents outside of the dead zone. The measured delay for transitions to 0 mA is 0.17 s. To incorporate this into the model and maintain continuous behaviour, a fourth-degree polynomial is fitted to the dead zone, with a value of 0.17 s at 0 mA and a smooth transition at the boundaries of the dead zone. The smooth transition is obtained by taking into account the function value and its derivation at the boundaries. A polynomial of degree four yields the most accurate fitting results.

3.3. Model evaluation

With adding random Gaussian noise to both models, which has similar characteristics as the position sensor of the rear-axle steering (max. 0.1 °), simulation results presented in **Figure 10** and **Figure 11** are obtained for a step and sinusoidal input signal. The simulated results are compared to the measurement of the real steer plant again with lifted tractor rear axle.

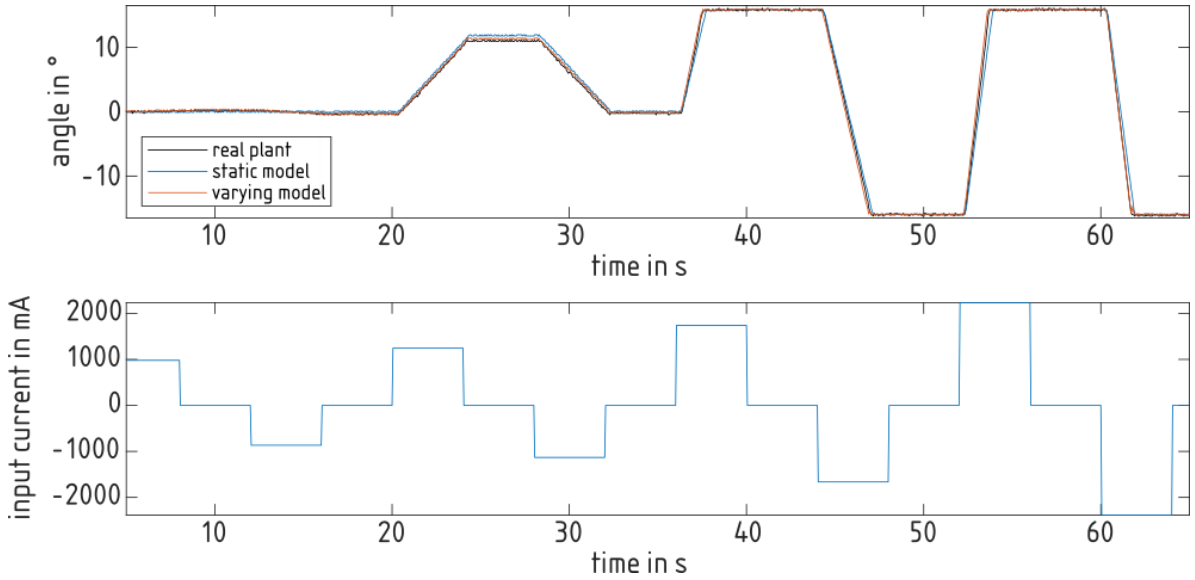

Figure 10: Simulation results for static and varying model for different step inputs

It can be observed that the model incorporating varying delay and varying time constant (section **3.2**) approximates the real steer process with better accuracy. This is particularly noticeable during the

step input signal for low currents, as well as during transitions to a 0 mA current when the steering angle is not restricted.

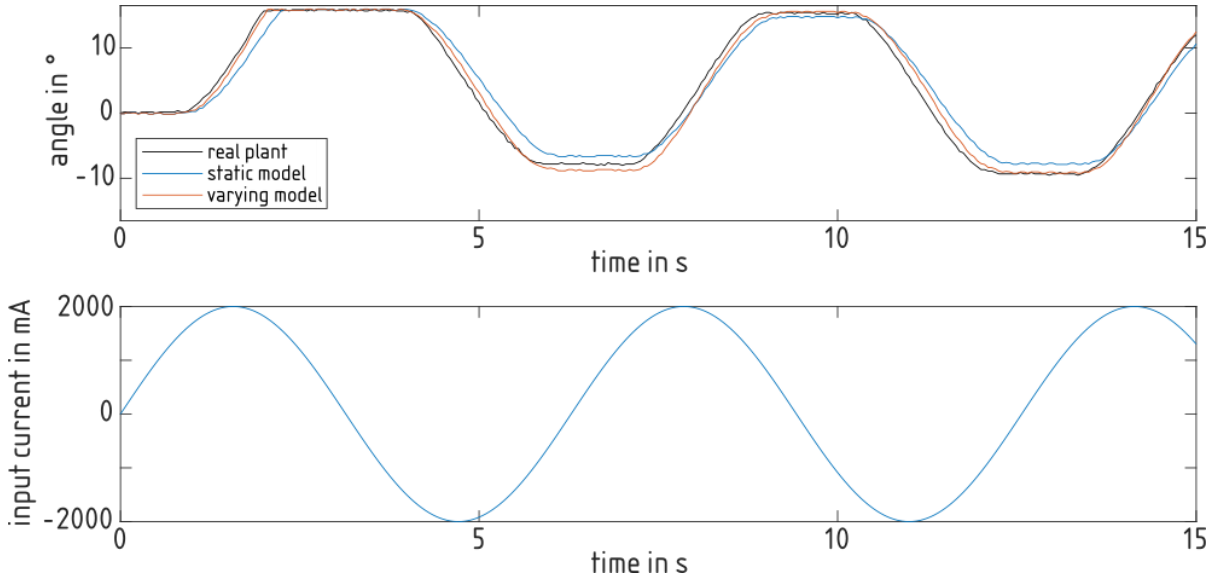

Figure 11: Simulation results for static and varying model for sinusoidal input

4. CONTROLLER DESIGN

In the following subsections, the architecture and parameter determination of different controllers is presented. There are: a PD controller tuned with FOLIPD tuning rules, a 2DOF state space controller combined with PD control and a PD gain scheduling controller.

To obtain a smoother feedback signal, a linear Kalman filter is utilized due to the presence of significant noise in the input signal received from the sensor, as presented in **Figure 12**.

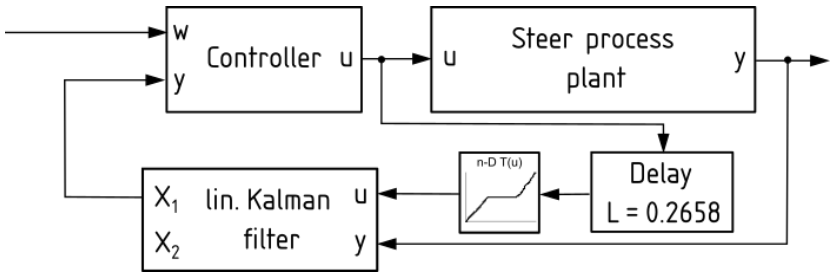

Figure 12: Implementation of Kalman filter to the steer process

Whereby set point w is steer angle, the control variable u is current and feedback y is the measured steer angle. The model of the Kalman filter is in a continuous state space representation (4) with the states position (X_1) and velocity (X_2):

$$A = \begin{pmatrix} 0 & 1 \\ 0 & -1/0.0385 \end{pmatrix}, b = \begin{pmatrix} 0 \\ 1/0.0385 \end{pmatrix}, \quad c = \begin{pmatrix} 1 & 0 \end{pmatrix}. \tag{4}$$

The nonlinear process gain (**Figure 6**), which accounts for the nonlinear behavior and dead zone, has been incorporated as a cascade block preceding the linear Kalman filter in order to accurately capture these characteristics. Additionally, to account for the delay introduced by the steer plant, a delay approximation has been incorporated before the Kalman filter (**Figure 12**).

4.1. PD controller based on FOLIPD tuning rules

Eriksson and Oksanen [4] propose a robust linear PID controller for FOLIPD processes with

unknown varying delay. Their proposed tuning rules are:

$$k = \frac{10^{f(L,T_F)}}{K_v L}, k_i = 0, k_d = \frac{T_F^{g(L,T_F)}}{K_v} 10^{h(L)}, \tag{5}$$

where

$$\begin{aligned} f(L,T_F) &= 0.0027\left(\frac{T_F}{L}\right)^2 - 0.0794\frac{T_F}{L} - 0.34, \\ g(L,T_F) &= 0.02 + (0.51 - 0.076\log_{10}(T_F))L^{0.15}, \\ h(L) &= 0.97 - 1.48\,L^{0.15}. \end{aligned} \tag{6}$$

The PID controller becomes effectively a PD controller and is to be used as a linear controller. For our PD controller, (5) and (6) result in $k = 1.6749$ and $k_d = 0.1029$, while $K_v = 1$. In order to obtain a linear process with $K_v = 1$, the nonlinear process gain (**Figure 6**) is compensated with its inverse function shown in **Figure 13** as proposed in [6, 8]. In order to obtain a bijective function, which is necessary for stability reasons, the function is modified around the zero-crossing.
Figure 14 depicts the integrated inverse element and the full architecture of the PD controller.

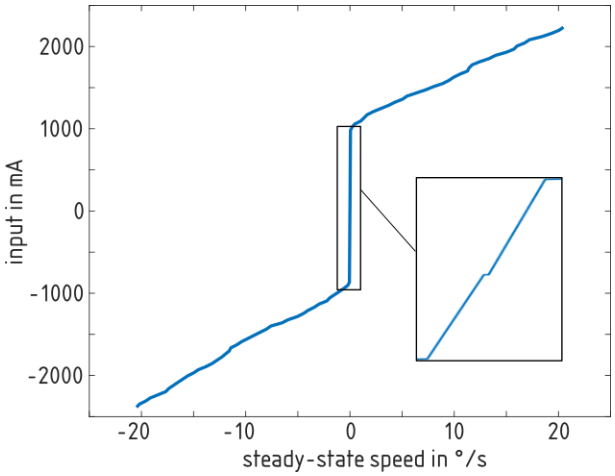

Figure 13: Inverse of nonlinear process function

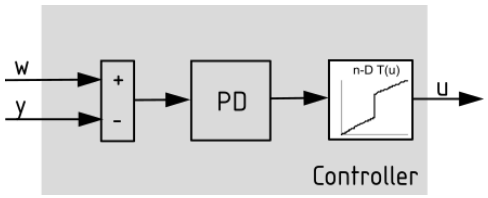

Figure 14: Architecture of PD Controller

4.2. Two degree of freedom state space controller combined with PD control

A second controller structure which has been studied is a 2DOF state space controller combined with a PD controller, presented in **Figure 15**:

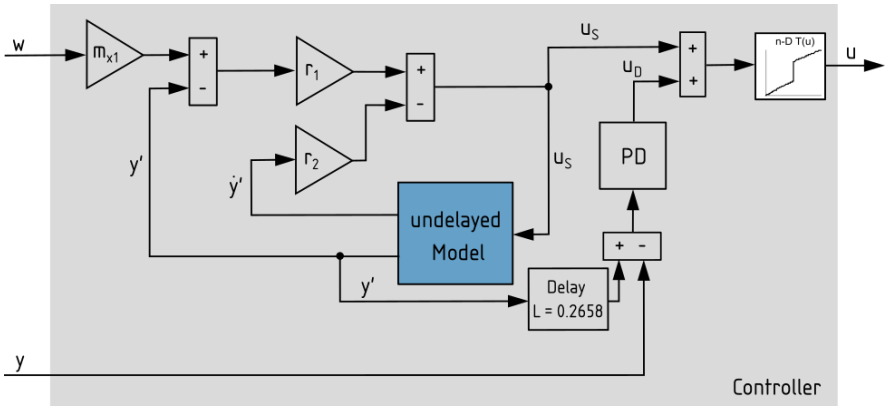

Figure 15: Architecture of 2-DOF controller comprising state space and PD controller

The state space controller exclusively operates on the undelayed model. For this, the model described in section **3.1** is utilized, omitting the delay. However, to address the discrepancy arising from the delay between the actual plant and the undelayed model, a PD controller, identical to the one

described in section **4.1**, is employed. The combination of both control signals is then adjusted with the inverse element explained in section **4.1**, ultimately yielding the control signal required for the steer plant.

According to Föllinger [9] the controller parameters are determined with (7-11). m_{x1} is calculated by applying (7):

$$\begin{pmatrix} m_{x1} \\ m_{x2} \\ m_u \end{pmatrix} = \begin{pmatrix} A & b \\ c^T & 0 \end{pmatrix}^{-1} \begin{pmatrix} 0 \\ I \end{pmatrix} = \begin{pmatrix} 1 \\ 0 \\ 0 \end{pmatrix}, \tag{7}$$

with

$$A = \begin{pmatrix} 0 & 1 \\ 0 & -1/0.0385 \end{pmatrix}, b = \begin{pmatrix} 0 \\ 1/0.0385 \end{pmatrix}, \tag{8}$$
$$c = \begin{pmatrix} 1 & 0 \end{pmatrix}.$$

The controller values r^T are calculated using following equations and pole placement [9]:

$$(s - \lambda_{R1}) \dots (s - \lambda_{Rn}) = s^n + p_{n-1}s^{n-1} + \dots + p_0 \tag{9}$$

$$t_1^T = e_n Q_s^{-1} \tag{10}$$

$$r^T = p_0 t_1^T + p_1 t_1^T A + \dots + p_{n-1} t_1^T A^{n-1} + t_1 A^n \tag{11}$$

Where λ are the Eigenvalues of the closed loop control system of the model, and Q_s the controllability matrix. In our case $n = 2$ is valid. From tuning, it resulted that with $\lambda_{R1} = -3.3$ and $\lambda_{R2} = -50.0$ the best control results are obtained.

4.3. Gain scheduling PD controller

A third controller for FOLIPD processes with time-varying gain, delay and time constant being tested, as described in the introduction, is a gain scheduled controller. Gain scheduling is commonly used for controlling nonlinear processes. The classical gain scheduling approach uses a family of controllers for multiple operating points [10]. An observable scheduling variable is used to determine the right linear controller depending on the operating point.

However, in our process, the only feedback available is the steering angle signal, which is not suitable as a scheduling variable, because of the integrator. Since the varying transfer function parameters, e. g. delay, are dependent on the actual current applied to the valve, the valve current control signal is used as scheduling variable, which results in an inherent problem. To overcome this, we propose below a procedure to determine the most appropriate controller for each operating point, despite the inherent problem.

For the controller design, a family of proportional gains k and the derivative gains k_d depending on the valve input current u_{sv} (scheduling variable) are calculated from (5). In our case, we used 100 different tuning sets for the PD controller. This represents a compromise between accuracy and the required computing power. The parameters for gain, time constant and delay result from the model described in section **3.2**.

The controller itself is then structured as follows:

1. Calculation of a vector of theoretically resulting valve input currents u_{th} based on the error e between the setpoint and feedback:

$$u_{th} = ke + k_d\dot{e} \tag{12}$$

2. u_{isp} results from finding the intersection point between u_{sv} and u_{th}.
3. To compensate dead zone and saturation, the following filter is applied:

$$u(t) = \begin{cases} u_{max}, & if\ u_{isp} > u_{max} \\ u_{isp}, & if\ u_{dz,+} \leq u_{isp} \leq u_{max} \\ u_{dz,+}, & if\ 0 < u_{isp} < u_{dz,+} \\ 0, & if\ u_{isp} = 0 \\ u_{dz,-}, & if\ u_{dz,-} < u_{isp} < 0 \\ u_{isp}, & if\ u_{min} \leq u_{isp} \leq u_{dz,-} \\ u_{min}, & if\ u_{isp} < u_{min} \end{cases} \quad (13)$$

With u_{max} being positive saturation limit, u_{min} negative saturation limit, $u_{dz,+}$ positive dead zone limit and $u_{dz,-}$ negative dead zone limit.

The controller gain tuning sets vary for k between roughly 160 and 8700 and for k_d between 8 and 1700. Results showed that the controller performance increases with higher values for the controller gains. Hence, k is multiplied by a factor of 1.3 and k_d by 1.4.

5. SIMULATION AND MEASUREMENT RESULTS

The controllers were implemented to the IQAN using the Simulink export for IQANdesign. In the following the control results from simulation and measurement are presented. **Figure 16** depicts the results for step responses with the varying simulation model described in section **3.2**.

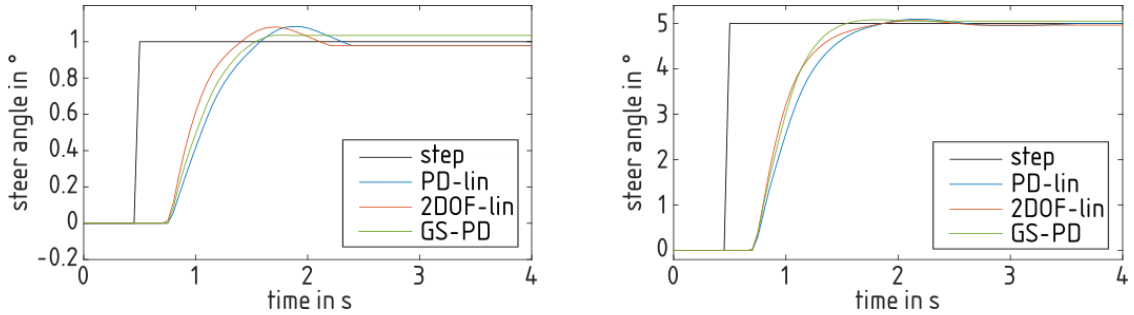

Figure 16: Step responses of controllers with varying simulation model from section 3.2

The PD controller and 2DOF controller with a linearized plant demonstrate superior steady-state accuracy, with $e_\infty = -0.02\,°$, when compared to the gain scheduling PD controller with $e_\infty = 0.03\,°$ for a step of 1 °. However, when it comes to overshoot, the gain scheduling controller outperforms the others. In terms of rise time, the 2DOF controller proves to be the fastest for a step of 1°, while the gain scheduling controller exhibits less rise time for a step of 5 °. The gain scheduling controller excels in terms of settling time for both steps.

When adding noise to the simulation model, especially the overshoot criteria changes for all of the controllers as shown in **Figure 17**.

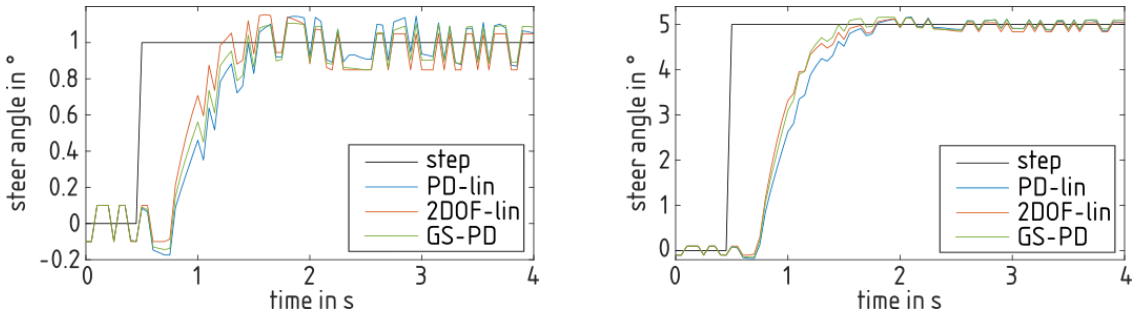

Figure 17: Step responses of controllers with varying noisy simulation model from section 3.2

Figure 18 depicts the unfiltered results obtained when the controllers are implemented to the actual plant. The PD controller outperforms the others in both step scenarios, although no noticeable distinction can be observed between the controllers. For a step of 1 ° the 2DOF controller shows higher rise time especially compared to the pure PD controller.

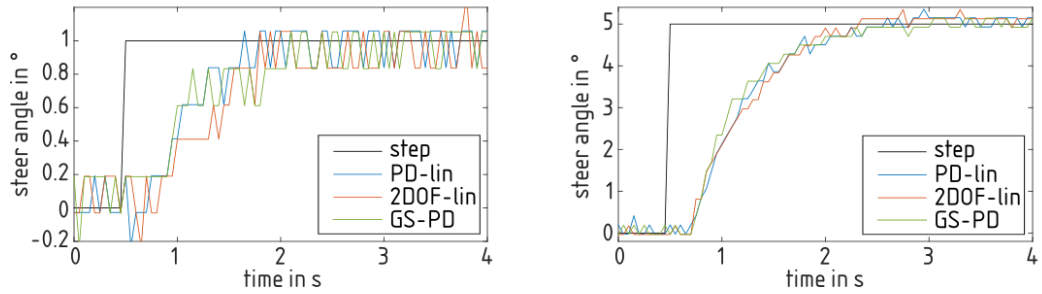

Figure 18: Measured unfiltered step responses of controllers at true steer plant

Figure 19 presents the comparison between simulation and measurement for the step responses of the gain scheduling PD controller. The difference in response time between the true plant and the noisy model is evident. Although the model exhibits some slight overshooting, such behavior is not observed in the measured data. This suggests that the controllers for the true plant could potentially be designed to operate even faster.

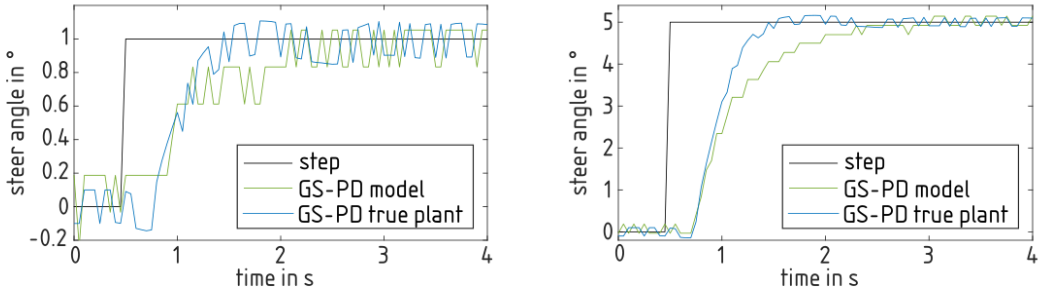

Figure 19: Simulated versus measured step responses (unfiltered) for gain scheduling PD control

Controller performance parameters are summarized in **Table 1** for the simulated response and **Table 2** for the measured response.

Table 1: Controller performance parameters from simulation with time-varying model without noise

Controller at step	Overshoot [%]	Settling time [s]	e_∞ [°]
PD-lin at 1 °	10.8	2.32	-0.022
2DOF-lin at 1 °	10.4	2.12	-0.021
GS-PD at 1 °	0.2	1.58	0.035
PD-lin at 5 °	1.9	1.72	0.002
2DOF-lin at 5 °	2.0	2.19	0.034
GS-PD at 5 °	0.6	1.49	0.050

Table 2: Controller performance parameters measured at true plant

Controller at step	Overshoot [%]	Settling time [s]	e_∞ [°]
PD-lin at 1 °	0.0	1.63	-0.086
2DOF-lin at 1 °	0.0	1.71	-0.146
GS-PD at 1 °	0.0	2.05	-0.080
PD-lin at 5 °	0.0	2.55	-0.006
2DOF-lin at 5 °	0.0	2.32	-0.218

GS-PD at 5 °	0.0	2.45	0.000

6. CONCLUSION AND OUTLOOK

To conclude, this paper presents two modelling approaches, with the new proposal containing varying delay and time constant proving to be better than the one with constant delay and time constant. In simulation, the gain scheduling exhibits the best results. However, in measurement scenarios, all controllers are operating similarly, with the PD controller and linearized plant performing slightly better than the others. All the controllers are stable.

It is worth mentioning that the model itself can still be improved. Furthermore, by utilizing a better model, the controllers can be made faster since the controllers highly rely on the accuracy of model parameters. Especially the gain scheduling controller could be improved with dedicated tuning rules.

Looking ahead, future research can focus on enhancing the proposed model and exploring alternative methods for improving controller performance, allowing for even more efficient and reliable control systems.

For our research tractor all the three presented control algorithms compensate system nonlinearities and provide smooth actuation of the rear-axle steering. Hence, all of them could be used for the "AMX G-trac" in future autonomous operation.

REFERENCES

[1] W. J. Thayer (1958 (revised in 1965)) Transfer function for MOOG servovalves. Controls Division, East Aurora, NY. technical bulletin

[2] Moosavi H, Mirza Hessabi R, Mercan O (2015) Numerical simulation and analysis of nonlinear state-space control design for hydraulic actuator control. Struct Control Health Monit 22:1068–1085. https://doi.org/10.1002/stc.1731

[3] Krata D, Ochman M, Panek M et al. (2021) Adaptive Smith Predictor Control Scheme for a Nonlinear Hydraulic System. In: 2021 26th IEEE International Conference on Emerging Technologies and Factory Automation (ETFA). IEEE, pp 1–6

[4] Eriksson L, Oksanen T, Mikkola K (2009) PID controller tuning rules for integrating processes with varying time-delays. Journal of the Franklin Institute 346:470–487. https://doi.org/10.1016/j.jfranklin.2009.01.003

[5] Możaryn J, Winnicki A, Suski D (2019) Impulse Identification and Discrete P/PD Control of Electro-Hydraulic Servodrive. JAMRIS 12:51–57. https://doi.org/10.14313/JAMRIS_4-2018/25

[6] Oksanen T (2010) Closed loop control over ISO 11783 network – challenges of plug-and-play. IFAC Proceedings Volumes 43:203–208. https://doi.org/10.3182/20101206-3-JP-3009.00035

[7] Galuppini G, Magni L, Raimondo DM (2018) Model predictive control of systems with deadzone and saturation. Control Engineering Practice 78:56–64. https://doi.org/10.1016/j.conengprac.2018.06.010

[8] Deng W, Yao J, Ma D (2017) Robust adaptive precision motion control of hydraulic actuators with valve dead-zone compensation. ISA Trans 70:269–278. https://doi.org/10.1016/j.isatra.2017.07.022

[9] Föllinger O (2022) Regelungstechnik. VDE Verlag

[10] Leith DJ, Leithead WE (2000) Survey of gain-scheduling analysis and design. International Journal of Control 73:1001–1025. https://doi.org/10.1080/002071700411304